



# Synchronous low frequency earthquakes and implications for deep San Andreas Fault slip



Daniel T. Trugman<sup>a,b,\*</sup>, Chunquan Wu<sup>a,c</sup>, Robert A. Guyer<sup>a,d</sup>, Paul A. Johnson<sup>a</sup>

<sup>a</sup> Geophysics Group (EES-17), Los Alamos National Laboratory, Los Alamos, NM 87545, USA

<sup>b</sup> Institute for Geophysics and Planetary Physics, Scripps Institution of Oceanography, San Diego, CA, USA

<sup>c</sup> Center for Earthquake Research and Information, University of Memphis, Memphis, TN, USA

<sup>d</sup> Department of Physics, University of Nevada, Reno, NV, USA

## ARTICLE INFO

### Article history:

Received 1 January 2015

Received in revised form 17 May 2015

Accepted 18 May 2015

Available online xxxx

Editor: B. Buffett

### Keywords:

low frequency earthquakes

lower crustal deformation

acoustic emission

Parkfield seismicity

earthquake clustering

## ABSTRACT

Low Frequency Earthquakes (LFEs) are slip events that occur repeatedly at source locations within the lower crust. LFEs, and the associated seismic broadcast known as tremor, have been observed in a diverse array of tectonic environments. Here we develop a suite of statistical tools to conduct a systematic study of the spatial and temporal correlations of the event occurrence patterns of the 88 LFE sources beneath the greater Parkfield section of the San Andreas Fault. We first examine correlations in the occurrence patterns on long time scales to show that the regions to the north and south of Parkfield behave independently. We next use the cumulative event signatures of each source to characterize the individual occurrence patterns on shorter time scales. Through application of a statistical clustering algorithm, we demonstrate that individual LFE sources form spatially coherent clusters that may represent localized elastic structures or asperities on the deep fault interface. We conclude by examining the fine-scale features of the event rates within the LFE occurrence patterns. Through quantitative comparison to analogous laboratory shear experiments on granular, fault gouge-like materials, we infer that the distinctive features of LFE occurrence patterns reflect variations in the in-situ stress and frictional conditions at the individual LFE source locations. These observations provide a framework to understand the spatial and temporal diversity of fault slip that occurs within the lower crust beneath Parkfield and that may influence seismic hazard in the region.

© 2015 Elsevier B.V. All rights reserved.

## 1. Introduction

The largest and most damaging earthquakes typically occur in the upper crust, where the frictional regime is primarily brittle. Yet knowledge of the upper crust is not in itself sufficient to characterize seismic hazard, as lower crustal slip beneath the seismogenic zone can drive the seismicity in the upper crust (Tse and Rice, 1986; Scholz, 2002) and lead to the nucleation of large earthquakes (Nadeau and Guilhem, 2009; Shelly, 2009; Segall and Bradley, 2012). Low Frequency Earthquakes (LFEs), which accompany the slow slip events observed on the deep extension of fault interfaces in Cascadia (Rogers and Dragert, 2003; Bostock et al., 2012), Japan (Obara et al., 2004; Shelly et al., 2006), and Mexico (Rivet et al., 2011; Frank et al., 2013), have also been observed

\* Corresponding author at: Institute for Geophysics and Planetary Physics, Scripps Institution of Oceanography, 9500 Gilman Drive, La Jolla, CA 92093-0225, USA. Tel.: +1 858 534 1927.

E-mail address: dtrugman@ucsd.edu (D.T. Trugman).

<http://dx.doi.org/10.1016/j.epsl.2015.05.029>

0012-821X/© 2015 Elsevier B.V. All rights reserved.

in the Parkfield region of California (Nadeau and Dolenc, 2005; Shelly et al., 2009), and present the opportunity to illuminate the elusive elastic and slip behaviors of the lower crust (Rubinstein et al., 2010).

Low Frequency Earthquakes differ from classical earthquakes in their relative deficiency in high frequency seismic radiation and in their location in the lower crust. Shelly and Hardebeck (2010) identified 88 LFE sources in the Parkfield region of California (Fig. 1) by cross-correlating template waveforms with the continuous seismic recordings at multiple High Resolution Seismic Network (HRSN) stations. The seismic events associated with each LFE source occur repeatedly at average rates that vary from source to source and range from ~300 to 3000 events per year. LFE events at a given source tend to occur in burst-like sequences of multiple events in rapid succession, generating a nearly continuous seismic broadcast known as tectonic tremor (Shelly et al., 2007). Though the focus of this study is on the occurrence patterns of individual LFE events, we note that LFEs and tremor appear to be part of the same underlying phenomenon.

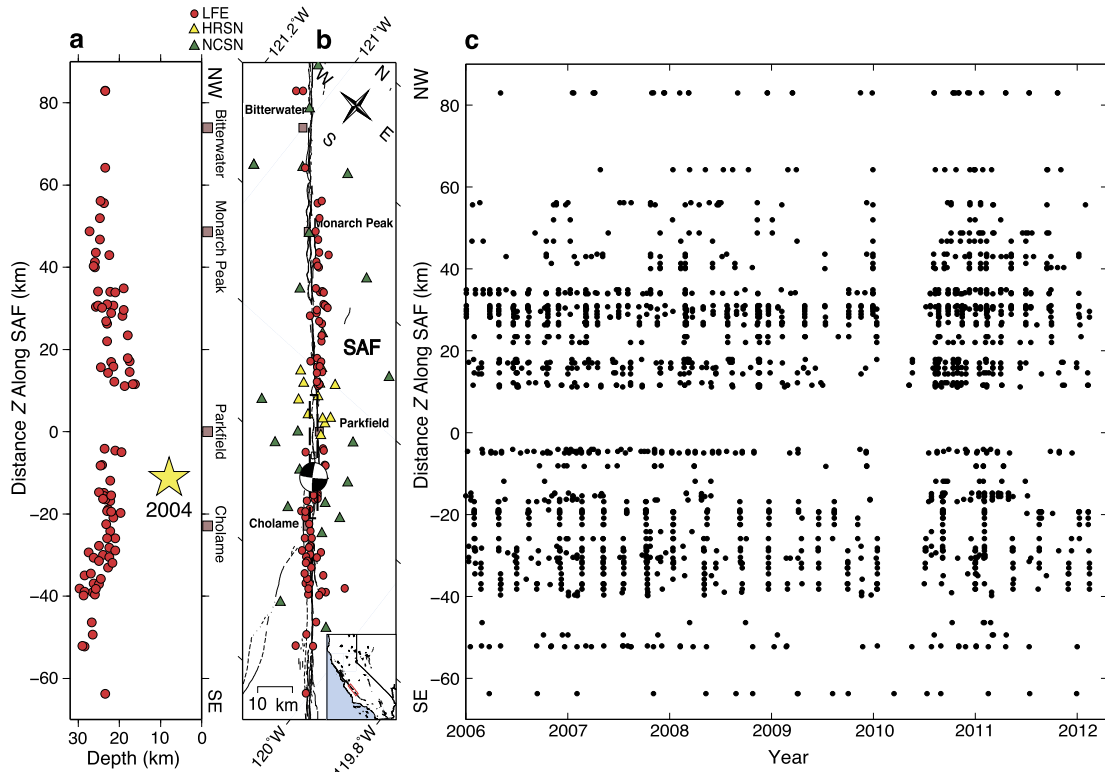


**Fig. 1.** Overview of the Parkfield study region and LFE seismicity. (a) Cross-sectional and (b) map view of the positions of the 88 LFE sources (red circles). The hypocentral position of the  $M_w$  6.0 2004 Parkfield earthquake is denoted in (a) with a yellow star. The locations of the HRSN and NCSN stations (yellow and green triangles, respectively), and the moment tensor solution and rupture zone for the 2004 Parkfield earthquake (Bennington et al., 2011), are shown in (b). (c) Space–time plot of the periods at which the LFE event rate exceeds 3 standard deviations above the mean rate. Each LFE source is displayed as function of along-strike source position  $Z$  from Parkfield ( $35.9^\circ\text{N}$ ,  $120.4^\circ\text{W}$ ;  $Z = 0$ ). (For interpretation of the references to color in this figure legend, the reader is referred to the web version of this article.)

The 2004  $M_w$  6.0 Parkfield earthquake transiently perturbed LFE activity in the region (Shelly and Johnson, 2011; Thomas et al., 2012; Wu et al., 2013). Consequently, we restrict our analysis to the 6+ year time interval  $T$  from January 1st, 2006 to February 1st, 2012. We use the comprehensive LFE catalog of Shelly and Hardebeck (2010), which consists of 88 sets of time points corresponding to the times of LFE event occurrence for each source. Each of the 88 LFE sources has a distinctive occurrence pattern, and we proceed under the premise that these patterns reflect the source's individual slip behavior.

In this study, we examine correlations in LFE occurrence patterns over multiple time and spatial scales. We first consider temporal correlations on timescales on the order of days – correlations that reveal a clear decoupling between the LFE sources located to the north of Parkfield from those to the south. We next characterize each individual LFE source using its cumulative event record, and compute what we term a *cumulative time signature* that quantifies the unique occurrence pattern of each source. By applying a statistical clustering algorithm to the individual cumulative time signatures, we find that the LFE sources at Parkfield naturally form spatially coherent patches, or *clusters*. These clusters contain sources with quantitatively similar occurrence patterns, and may represent coherent elastic structures or asperities on the deep fault interface. We conclude with an analysis of the spectrum of event rates exhibited within the occurrence patterns of each LFE source. Through quantitative comparison with laboratory shear experiments in fault gouge-like materials, we demonstrate that the variability in these event rate spectra is likely caused by differences in the stress and frictional conditions experienced by each LFE source.

## 2. Methods and results

### 2.1. Temporal correlations of periods of high LFE activity

We begin our examination of the space–time correlations in LFE occurrence patterns by tracking periods of time in which an individual source is particularly active. To accomplish this, we break the observation interval (a total of 2222 days from January 1st, 2006 to February 1st, 2012) into discrete, 2-day time bins, and for each source, form 1111-component vectors (i.e., one component per time bin) containing the count of the number of LFE events in each 2-day interval. To identify the periods of time in which each LFE source is particularly active, we form corresponding binary, 1111-component vectors in which the time bins with an event rate (events/time bin) greater than 3 standard deviations above the mean rate are given a value of one. All other time bins are given a value of zero. The values of mean and standard deviation in event rate are computed individually for each source.

To facilitate comparison of the vectors  $\{V_n\}$  for each of the  $n$  sources, we remove the mean component of each vector and normalize each vector to 1. In this way,  $V_i \cdot V_i = 1$  for any source  $i$ , and the inner product  $V_i \cdot V_j$  provides a quantitative measure of the temporal correlation of the periods of high LFE activity for any pair of sources  $i$  and  $j$ . We compute these pairwise correlation coefficients  $\rho_{ij} = V_i \cdot V_j$  for each of the 3828 possible LFE source pairs  $(i, j)$ .

We display the results of this analysis in Fig. 1c, in which the time bins corresponding to high LFE event rates are denoted with a dot. Each LFE source is sorted by its distance,  $Z$ , from Parkfield ( $35.9^\circ\text{N}$ ,  $120.4^\circ\text{W}$ ) along the strike of the SAF. The vertical streaking apparent in Fig. 1c (e.g., among sources located between

$Z = -20$  km and  $Z = -40$  km along strike) is evidence of correlation of high event rates for nearby sources. Strong spatiotemporal correlations are seen north and south of Parkfield ( $Z = 0$  km), but these correlations do not appear to extend across the notable gap in LFE sources at Parkfield.

We demonstrate this quantitatively by sorting the 3828 possible pairwise correlation coefficients ( $\rho_{ij} = V_i \cdot V_j$ ) into three groups: (1) the 1128 pairs where both sources reside to the south of Parkfield, (2) the 780 pairs where both sources reside to the north of Parkfield, and (3) the remaining 1920 pairs with a single source from both the north and south of Parkfield. The source pairs from group 1 (both south of Parkfield) exhibit strong temporal correlation: 28.5% of all possible group 1 source pairs have positive correlation coefficients that are statistically significant at the 99% confidence level (obtain via Monte Carlo simulation). Similarly, 34.7% of all possible group 2 source pairs (both north of Parkfield) exhibit statistically significant temporal correlation. In contrast, only 0.4% of the group 3 source pairs (mixed north-south) exhibit this same level of temporal correlation, indicating that the LFE sources north and south of Parkfield are essentially decoupled. This result is robust with respect to the length of the observation interval (i.e., time bin), effectively ruling out propagation of LFE activity across the Parkfield gap at the slow velocities ( $\sim 10$  km/day) observed in subduction zones (Obara et al., 2004; Wech and Creager, 2011).

Differences in LFE occurrence between the northern and southern sources have been observed in several previous studies. Shelly and Hardebeck (2010) found that the seismic amplitudes of the southern sources tend to be larger than the amplitudes of the northern sources. Guilhem and Nadeau (2012) found that the southern LFE sources participate in quasi-periodic tremor episodes. Likewise, differences in sensitivity to static stresses (Shelly and Johnson, 2011), dynamic stresses (Shelly et al., 2011), and tidal loading (Thomas et al., 2012) for the northern and southern sources have all been noted in previous studies. Our results provide additional evidence that the northern and southern segments of the deep San Andreas Fault behave independently.

## 2.2. Clustering of nearby LFE sources

We quantitatively characterize the distinctive features of the LFE event record of each source by computing what we term the *cumulative time signature* of each LFE source. There are three basic steps in forming the *cumulative time signature*,  $CTS(t)$ , for an individual LFE source (outlined pictorially in Fig. S1 in the supplementary material). We first compute  $N(t)$ , the fraction of LFE events occurring at or before time  $t$ . We then subtract a quadratic polynomial fit from  $N(t)$ , resulting in  $dN(t)$ . For this step, we use a quadratic (rather than linear) fit for the long-term trend because the event rate decreases as time advances; this slow decrease in event rate may be related to the long-term recovery process from the effects of the 2004  $M_w$  6.0 Parkfield earthquake (Shelly and Johnson, 2011; Wu et al., 2013). The final *cumulative time signature*,  $CTS(t)$ , is obtained by interpolating  $dN(t)$  to 8912 time points that are uniformly distributed over the observation interval  $T$ , removing the low-frequency Fourier components of  $dN(t)$  (those with periods greater than 100 days), and normalizing the resulting vector to 1.

The *cumulative time signature* provides a fingerprint that quantitatively represents the occurrence patterns of each LFE source over 6+ years from which the slowly varying, long-term trends have been removed (Fig. S2 in the supplementary material). Further, the  $CTS(t)$  allow for a quantitative comparison of the occurrence patterns among the sources. To measure the similarity between the occurrence patterns of two distinct LFE sources,  $m$  and  $n$ , we use the maximum value of the cross-correlation between the  $CTS(t)$ :

$$S_{mn} = \max_{\tau} \{ CTS_m(t) \cdot CTS_n(t + \tau) \} \quad (1)$$

Pairs of sources with similar occurrence patterns have a higher  $S$  than those with less similar occurrence patterns, with  $S$  approaching one in the limit that the patterns are identical (i.e.,  $S_{nn} = 1$  for all  $n$ ).

Previous studies have hinted at the possibility that certain groups of nearby sources tend to exhibit qualitatively similar occurrence patterns (Shelly, 2010b; Guilhem and Nadeau, 2012). The cumulative time signatures we develop enable us to rigorously assess this observation through a statistical analysis of the spatial correlations of the LFE occurrence patterns. To this end, we use a hierarchical clustering algorithm (Kaufmen and Rousseeuw, 2005) to sort the sources into *clusters* based on the similarity of their cumulative time signatures (equation (1)). Sources within a given cluster therefore have occurrence patterns that are quantitatively similar in form. We iterate the clustering algorithm until we obtain clusters whose individual sources have a similarity  $S$  of at least 0.8 with the mean cumulative time signature for the cluster. A range of similarity thresholds were tested, and 0.8 was chosen based upon visual inspection of the similarity of the individual  $CTS(t)$  within each cluster. The clustering results are not highly sensitive to the choice of threshold. Note that with this threshold, some sources comprise their own distinct cluster: they do not have a  $CTS(t)$  that is similar enough to the  $CTS(t)$  of any other source to be joined in a cluster with another source.

The results of the clustering procedure are displayed in Fig. 2a (south) and 2b (north). The clusters of LFEs with synchronous occurrence patterns tend to be grouped in space, suggesting the identification of coherent structures or localized asperities on the deep fault interface that share the same elastic response to tectonic forcing or transient pulses of slow slip. Furthermore, the dominant orientation of the clusters changes as one moves north to south. The clusters to the north of Parkfield tend to be vertical structures, while the clusters to the south tend to be more extensive in the horizontal direction. Cluster 1S, for example, extends more than 40 km along strike.

The clusters themselves are not entirely independent. A measure of the coupling between clusters can be found by computing the mean, or *template* cumulative time signature for each cluster (Fig. 2c). By calculating the correlation between the template cumulative time signatures of different clusters we obtain a matrix of cluster correlation coefficients (Fig. S3 in the supplementary material) that provides a quantitative measure of the relative strength of coupling between distinct clusters.

Our results are consistent with and complementary to the recent study of Shelly (2015), who used a cross-correlation analysis of the source event record to investigate the tendency for LFE activity to migrate from source to source at velocities of order 50 km/h. As one might expect, the sources within each LFE cluster we identify tend to have strong migration connections as measured by Shelly (2015). The key difference between our study and that of Shelly (2015) is the timescale relevant to each analysis. By comparing LFE occurrence patterns at timescales longer than the timescale of order minutes in Shelly (2015), we lose the temporal resolution necessary to study pairwise migration patterns, but improve our ability to identify clusters of coupled LFE sources.

The spatial clustering of LFE sources at Parkfield is reminiscent of observations of segmentation of tremor sources in subduction zones (Brudzinski and Allen, 2007; Obara, 2010). This suggests that there may be certain universal features, like the spatial clustering of sources on coherent elastic structures and the tendency for LFE and tremor activity exhibit spatial migration (Rogers and Dragert, 2003; Obara et al., 2004), that typify deep crustal deformation and slow slip in all tectonic settings.

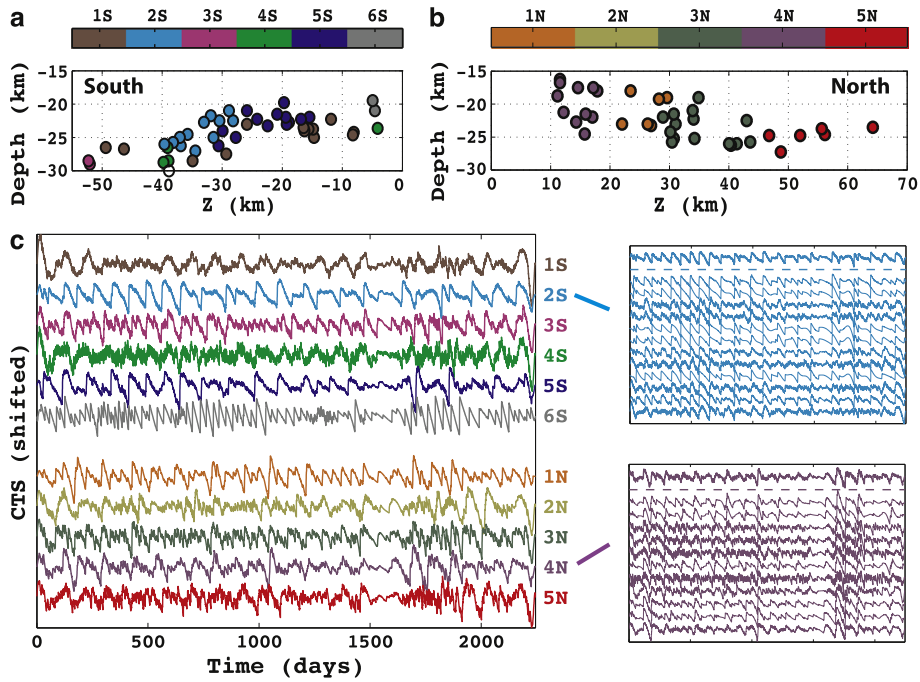


**Fig. 2.** LFE cluster locations and template cumulative time signatures. (a) Positions of the 48 LFE sources south of Parkfield. The LFE sources are color-coded by cluster, and markers without coloration correspond to LFE sources that do not belong to a cluster. (b) Similar to panel (a), but for the 40 LFE sources north of Parkfield. (c) Template cumulative time signatures for all LFE clusters. The individual cumulative time signatures for all sources in clusters 2S and 4N are shown as examples in the inset and are separated from the template signature by a dotted line.

### 2.3. Continuous and episodic styles of LFE occurrence

The diversity in the forms of the cumulative time signatures makes it apparent that different LFE sources can have markedly different *styles* of occurrence pattern. As noted by Shelly (2010a) the event rate of some LFE sources is fairly consistent over time (e.g., Fig. 3a, bottom), while for others, LFE event rates are highly episodic, with burst-like sequences of LFE events separated by long quiescent periods (e.g., Fig. 3a, top). To quantify the style of LFE occurrence for individual sources, we compute the coefficient of variation in the daily event rate  $r$ :

$$COV_r = \frac{std(r)}{mean(r)} = \frac{\sqrt{E[r^2] - E[r]^2}}{E[r]} \quad (2)$$

Since  $COV_r$  is simply the standard deviation in  $r$  divided by the mean  $r$  (for each source), LFE sources with continuous occurrence styles have low  $COV_r$ , while those with episodic occurrence styles have high  $COV_r$  (Fig. 3b).

The LFE sources appear to evolve from *episodic* (high  $COV_r$ ) to *continuous* (low  $COV_r$ ) with depth (Fig. 3). This finding is consistent with the observations of Shelly and Johnson (2011), who use an analogous statistical metric (termed *MFD75*) to quantify the occurrence style of LFE sources. The primary advantage of our  $COV_r$  metric is its generality: it can be applied to compare episodicity of repeating signals in a variety of contexts, independent of the background event rate. We demonstrate such an application to laboratory shear experiments in Section 3.

Using the  $COV_r$  metric, we find that nearby LFE sources tend to have similar styles of LFE occurrence (Fig. 3). There are, however, marked differences between the sources to the north and south of Parkfield. Namely, the southern LFE sources are bimodal – either highly episodic or highly continuous – while the northern LFE sources exhibit a broader spectrum of occurrence styles between these two limiting cases. Furthermore, while most clusters contain LFE sources with predominantly the same style of occurrence (e.g., clusters 4N and 1S), several of the larger clusters (e.g., 2S) contain

sources with diverse occurrence styles (Fig. S3 in the supplementary material).

### 3. Discussion: recurrence spectra of LFE sources and comparison to laboratory shear experiments

These systematic differences in the styles of LFE occurrence are intriguing, and motivate a closer examination of the fine features of the occurrence patterns of individual sources. For a source that has successive LFE events at times  $t_m$  and  $t_{m+1}$ , we can define the *recurrence rate* at the mean event time,  $(t_m + t_{m+1})/2$ , to be the reciprocal of the *recurrence interval* between the two event times:  $1/(t_{m+1} - t_m)$ . In Fig. 4, we show the full spectrum of recurrence rates for two representative LFE sources with contrasting occurrence styles: episodic and continuous (these same sources are featured in Fig. 3).

The occurrence style of an individual source can be easily distinguished by examining its spectra of recurrence rates. The bursts of LFE activity associated with episodic sources (high  $COV_r$ ) have recurrence rate spectra that are self-similar in nature, with rates that span time-scales over 6 orders of magnitude. In contrast, the sources with continuous occurrence styles (low  $COV_r$ ) tend to have bimodal recurrence spectra and notably shorter maximum recurrence intervals.

We can gain insight into the physical processes underlying these differences in recurrence rate spectra through comparison to laboratory studies of shear slip in granular media under a variety of experimental conditions (Johnson et al., 2012, 2013, see Appendix A for further experimental details). In such studies, there is a clear transition from episodic to continuous occurrence of acoustic emission (slip events that we posit to be analogous to LFEs) with decreasing normal stress (Fig. 4, panels (e) and (f)). This transition corresponds to an evolution from an episodic, or *stick-slip-like*, slip regime to a continuous, or *stable-sliding* slip regime (Marone, 1998).

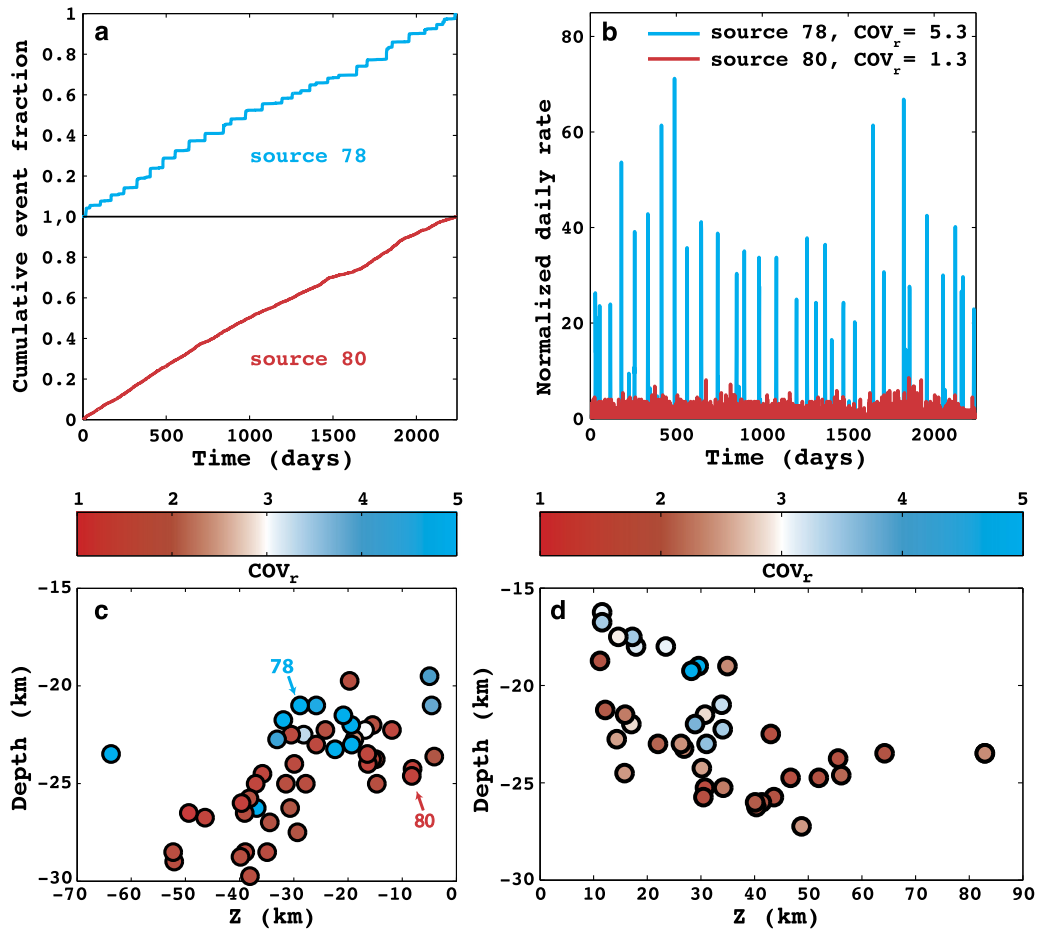


**Fig. 3.** LFE occurrence styles and event rate  $COV_r$ . (a) Comparison of the time evolution of the cumulative fraction of LFE occurrences at sources 78 and 80 (both located to the south of Parkfield). Source 78 has a highly episodic occurrence style, while source 80 has a highly continuous occurrence style. (b) Comparison of the daily event rate (normalized by the mean rate) for sources 78 and 80. (c) Rate coefficient of variation ( $COV_r$ ) for the LFE sources south of Parkfield, with source 78 and 80 labeled for reference. Cooler colors correspond to higher  $COV_r$ . The cross-section is exaggerated in the vertical direction for clarity. (d) Similar to (c), but for the LFE sources north of Parkfield.

We can quantify this observation more precisely by computing the coefficient of variation in the event rate of acoustic emission for laboratory experiments with different levels of applied normal stress (Fig. 5).  $COV_r$  for the laboratory data is computed in a similar fashion as for the LFE data set (equation (2)) except the rate of acoustic emission is computed in time bins of 0.25 s, instead of the daily time bins used for the LFE data set. The results are not highly sensitive to the choice of bin size – we use bins of 0.25 s for the laboratory data to ensure that we have approximately the same number of time bins for the computation of lab  $COV_r$  as we have for the computation of LFE  $COV_r$ .

The rheology and physical conditions of the deep SAF are undoubtedly more complex than that of the laboratory experiments. It is, however, plausible that many of the same physical processes that control the occurrence styles of acoustic emission in laboratory shear experiments (e.g., normal stress, shearing rate, and fault gouge composition) may be responsible for the distinctive features in the patterns of LFE occurrence. For example, LFE source regions where local fault conditions include lower effective stress (e.g., higher pore pressure) or more fine-grained (e.g., clay-like) fault gouge material would tend to exhibit continuous styles of LFE occurrence (i.e., a stable sliding regime). Source regions with higher effective stress or coarser gouge material would tend to exhibit episodic LFE occurrence (i.e., a stick-slip-like regime).

Laboratory shear experiments on granular, gouge-like materials also provide an intriguing analog to the natural occurrence of LFEs because of the importance of slip-induced dilatancy to the frictional dynamics in both contexts. In laboratory experiments, the fault gouge tends to dilate with increasing shear rate (Samuelson et al., 2009). Slip-induced dilatancy has likewise been hypothesized to be an important mechanism in regulating the frictional stability of slow slip and tremor (and hence, LFEs) within the earth (Segall et al., 2010; Shelly, 2015), as dilation reduces the pore pressure and therefore increases the effective normal stress on the fault interface.

We further note that the episodic LFE sources tend to be shallower than those with continuous occurrence styles (Figs. 3 and 5), suggesting an evolution from brittle, unstable slip behavior to ductile, stable slip behavior with depth. Similar observations have been documented in tremor zones of Japan (Obara et al., 2010) and Cascadia (Wech and Creager, 2011), and have broader implications for seismic hazard in the Parkfield region. The upper-crustal section of the SAF to the south of Parkfield is currently locked, having last ruptured during the 1857  $M_w$  7.9 Fort Tejon earthquake (Sieh, 1978). This locked section is situated directly above a cluster of LFE sources with episodic but quite frequent occurrence (Fig. 3). Slow slip transients in the deep fault system, through elastic coupling to the adjacent upper crust, may therefore load this locked section and play an important role in the nucleation of a future large earthquake (Shelly et al., 2007).

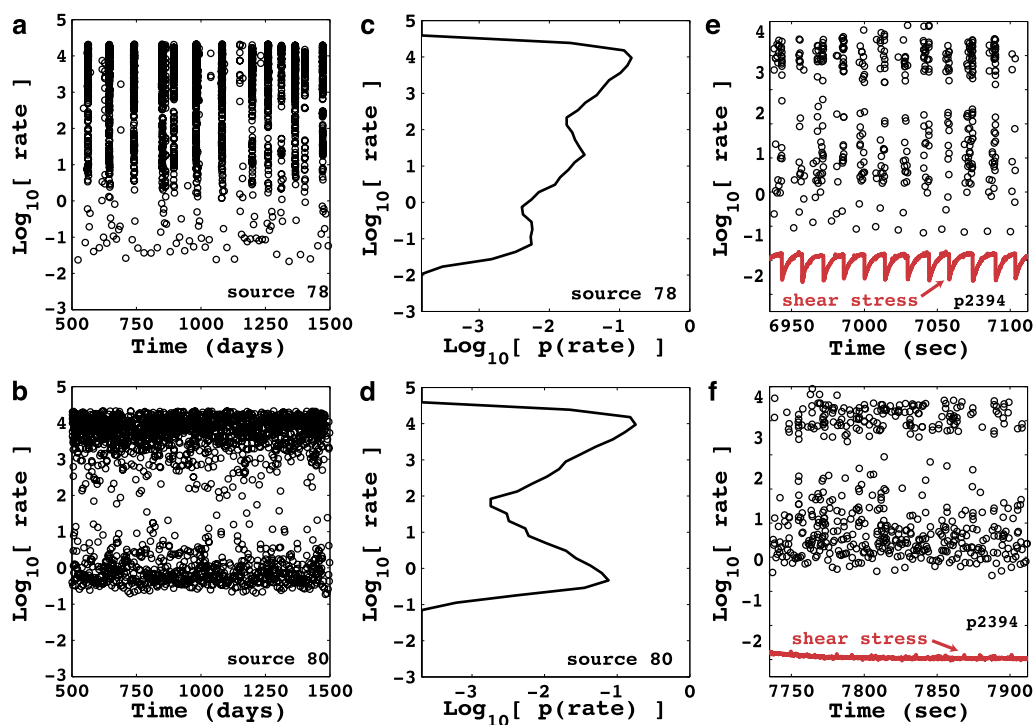


**Fig. 4.** Recurrence rate spectra. Logarithm of the recurrence rates for LFE sources 78 (a), and 80 (b), are plotted as a function of time for the time interval between 500 and 1500 days after January 1st, 2006. Source 78 has a highly episodic occurrence style, while source 80 has a highly continuous occurrence style. The corresponding probability density functions (log–log scale) for the entire observation time interval are shown in (c) and (d), respectively. Logarithm of the acoustic emission event recurrence rates are plotted for 3-minute time intervals of laboratory shear experiment p2394, with applied normal loads of (e) 5 MPa and (f) 3 MPa. Measured shear stress (arbitrary units) is plotted for reference. Note the strong correlation of acoustic emission with stress drop in (e).

#### 4. Conclusions

No geodetic signals from deep slow slip events have been directly observed along the Parkfield portion of the SAF (Johnston et al., 2006), though episodes of LFEs and tremor have been used to infer deep slow slip events reminiscent of ETS in Cascadia and Japan (Guilhem and Nadeau, 2012). Consequently, LFE sources and their associated occurrence patterns are important tools for probing the stress, frictional, and slip characteristics of the deep SAF. We have conducted a detailed statistical analysis of the patterns of LFE occurrence for 88 individual sources near Parkfield. Our analysis suggests that the regions to the north and south of Parkfield are decoupled. Each of these regions is assembled from discrete elastic structures or asperities in which clusters of LFE sources with similar occurrence patterns reside. These sources have distinctive, fine features in their occurrence patterns that can be characterized by their spectra of event occurrence rates. Guided by laboratory experiments, we posit that these fine features reflect the slip and stress conditions at the LFE source locations. The resulting map of slip and stress conditions revealed through our multiscale analysis of LFE occurrence patterns provides a basis for assessing deformational processes in the deep SAF.

#### Acknowledgements

The LFE data used for this work was derived from the updated LFE catalog maintained by David Shelly (Shelly and Hardebeck, 2010). Data from laboratory slip experiments was obtained and used with permission from Paul Johnson (Johnson et al., 2013). Both data sets may be accessed by contacting the corresponding author directly.

This research was supported by Institutional Support at Los Alamos National Laboratory, and is based upon work supported by the National Science Foundation Graduate Research Fellowship Pro-

gram (NSFGRFP) under grant number DGE-1144086. Discussions with W. Frank, A. Delorey, J. Gomberg, and D. Shelly helped to guide this study. We are also grateful for the thoughtful reviews provided by A. Thomas, an anonymous reviewer, and the Editor, all of which greatly improved the manuscript.

#### Appendix A. Description of laboratory acoustic emission experiments

The acoustic emission (AE) recurrence data used for this study comes from double-direct shear experiments (Marone, 1998) using a servo-hydraulic testing machine (Johnson et al., 2012, 2013). Our analysis of AE recurrence rates is based on experiment p2394 (Johnson et al., 2013), in which two layers of simulated fault gouge were subjected to a shear stress using a double-direct shearing apparatus. The simulated fault gouge consisted of class IV spheres (with dimensions from 105–149  $\mu\text{m}$ ), with initial layer thicknesses of  $2 \times 4$  mm (two layers). The drive block vertical displacement rate was 5  $\mu\text{m/s}$ , corresponding to a strain rate of approximately  $1.2 \times 10^{-3} \text{ s}^{-1}$ . The applied normal stress was incrementally increased from 2 MPa to 8 MPa and then decreased back to 2 MPa, in increments of 1 MPa. The time series of AE recurrence rate shown in Fig. 4e and Fig. 4f are from 3-min intervals from the downgoing stress steps in experiment p2394, with normal loads of 5 MPa and 3 MPa, respectively.

The shearing apparatus in experiment p2394 was servocontrolled so that constant normal stress and displacement rate of the drive block were maintained at  $\pm 0.1$  kN and  $\pm 0.1$   $\mu\text{m/s}$ , respectively. The shearing stresses were then measured with a strain gauge, and the loads, displacements and stresses were monitored by computer at 10 kHz sampling frequency. We also used another acquisition system to record the acoustic acceleration, shear stress and layer thickness at a sampling frequency of 330 kHz. Detailed experiment parameters can be found in (Johnson et al., 2013).

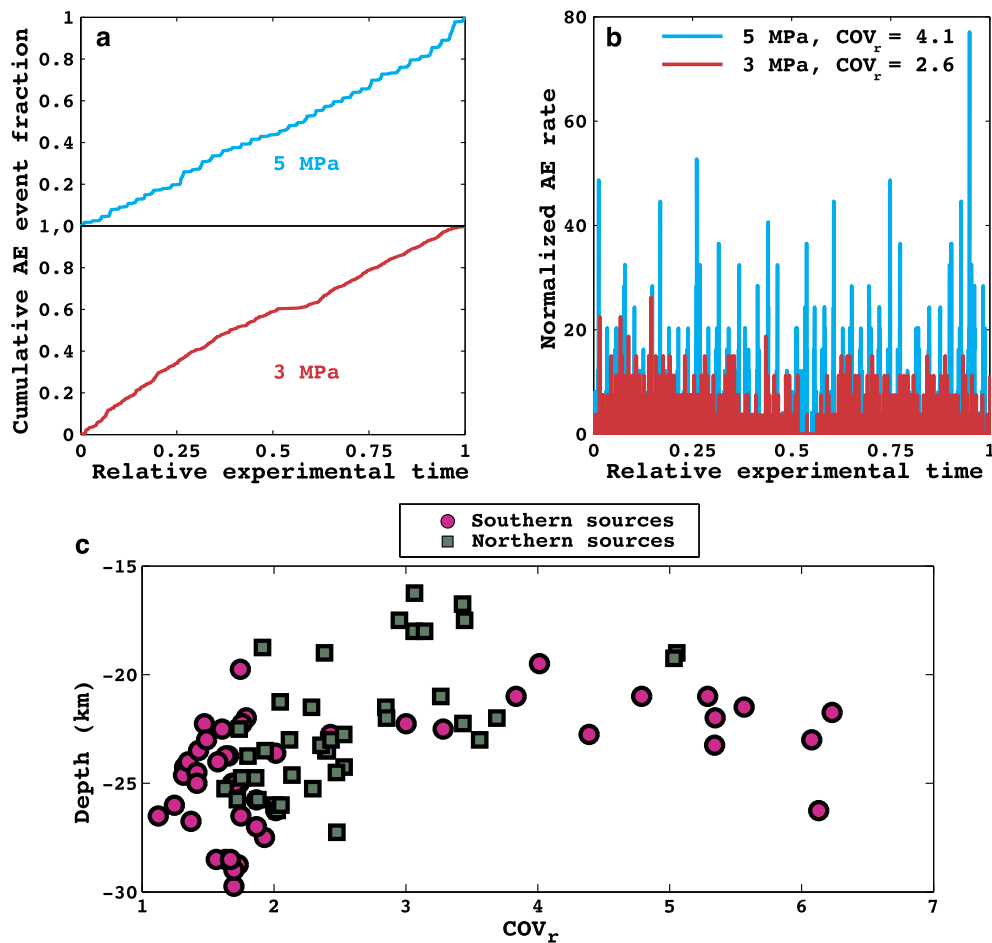


**Fig. 5.** Acoustic emission  $COV_r$  and depth-dependence of LFE  $COV_r$ . (a) Comparison of the time evolution of the cumulative fraction of acoustic emissions (AE) for laboratory shear experiments on granular media with 5 MPa (top) and 3 MPa (bottom) normal stress. (b) Comparison of the AE event rate (computed every 0.25 s, and normalized by the mean rate) for the same laboratory experiments. (c)  $COV_r$  as a function of depth for LFE sources south (pink circles) and north (green squares) of Parkfield. (For interpretation of the references to color in this figure legend, the reader is referred to the web version of this article.)

## Appendix B. Supplementary material

Supplementary material related to this article can be found online at <http://dx.doi.org/10.1016/j.epsl.2015.05.029>.

## References

- Bennington, N., Thurber, C., Feigl, K., Murray-Moraleda, J., 2011. Aftershock distribution as a constraint on the geodetic model of coseismic slip for the 2004 Parkfield earthquake. *Pure Appl. Geophys.* 168 (10), 1553–1565. <http://dx.doi.org/10.1007/s00024-010-0214-x>.
- Bostock, M.G., Royer, A.A., Hearn, E.H., Peacock, S.M., 2012. Low frequency earthquakes below southern Vancouver Island. *Geochem. Geophys. Geosyst.* 13 (11), Q11007. <http://dx.doi.org/10.1029/2012GC004391>.
- Brudzinski, M.R., Allen, R.M., 2007. Segmentation in episodic tremor and slip all along Cascadia. *Geology* 35 (10), 907–910. <http://dx.doi.org/10.1130/G23740A.1>.
- Frank, W.B., Shapiro, N.M., Kostoglodov, V., Husker, A.L., Campillo, M., Payero, J.S., Prieto, G.A., 2013. Low-frequency earthquakes in the Mexican Sweet Spot. *Geophys. Res. Lett.* 40 (11), 2661–2666. <http://dx.doi.org/10.1002/grl.50561>.
- Guilhem, A., Nadeau, R.M., 2012. Episodic tremors and deep slow-slip events in Central California. *Earth Planet. Sci. Lett.* 357–358 (0), 1–10. <http://dx.doi.org/10.1016/j.epsl.2012.09.028>.
- Johnson, P., Carpenter, B., Knuth, M., Kaproth, B., Le Bas, P., Daub, E., Marone, C., 2012. Nonlinear dynamical triggering of slow slip on simulated earthquake faults with implications to Earth. *J. Geophys. Res.* 117, B04310. <http://dx.doi.org/10.1029/2011JB008594>.
- Johnson, P.A., Ferdowsi, B., Kaproth, B.M., Scuderi, M., Griffa, M., Carmeliet, J., Guyer, R.A., Le Bas, P., Trugman, D.T., Marone, C., 2013. Acoustic emission and microslip precursors to stick-slip failure in sheared granular material. *Geophys. Res. Lett.* 40 (21), G1057848. <http://dx.doi.org/10.1002/2013GL057848>.
- Johnston, M.J.S., Borchardt, R.D., Linde, A.T., Gladwin, M.T., 2006. Continuous Borehole Strain and pore pressure in the near field of the 28 September 2004 M 6.0 Parkfield, California, Earthquake: implications for nucleation, fault response, earthquake prediction, and Tremor. *Bull. Seismol. Soc. Am.* 96 (4B), S56–S72. <http://dx.doi.org/10.1785/0120050822>.
- Kaufmen, L., Rousseeuw, P., 2005. *Finding Groups in Data: An Introduction to Cluster Analysis*. Wiley–Interscience, Indianapolis, IN.
- Marone, C., 1998. Laboratory-derived friction laws and their application to seismic faulting. *Annu. Rev. Earth Planet. Sci.* 26 (1), 643–696.
- Nadeau, R.M., Dolenc, D., 2005. Nonvolcanic tremors deep beneath the San Andreas Fault. *Science* 307 (5708), 389. <http://dx.doi.org/10.1126/science.1107142>.
- Nadeau, R.M., Guilhem, A., 2009. Nonvolcanic tremor evolution and the San Simeon and Parkfield, California, earthquakes. *Science* 325 (5937), 191–193. <http://dx.doi.org/10.1126/science.1174155>.
- Obata, K., 2010. Phenomenology of deep slow earthquake family in southwest Japan: spatiotemporal characteristics and segmentation. *J. Geophys. Res., Solid Earth* 115 (B8), B00A25. <http://dx.doi.org/10.1029/2008JB006048>.
- Obata, K., Hirose, H., Yamamizu, F., Kasahara, K., 2004. Episodic slow slip events accompanied by non-volcanic tremors in southwest Japan subduction zone. *Geophys. Res. Lett.* 31 (23), L23602. <http://dx.doi.org/10.1029/2004GL020848>.
- Obata, K., Tanaka, S., Maeda, T., Matsuzawa, T., 2010. Depth-dependent activity of non-volcanic tremor in southwest Japan. *Geophys. Res. Lett.* 37 (13), L13306. <http://dx.doi.org/10.1029/2010GL043679>.
- Rivet, D., Campillo, M., Shapiro, N.M., Cruz-Atienza, V., Radiguet, M., Cotte, N., Kostoglodov, V., 2011. Seismic evidence of nonlinear crustal deformation during a large slow slip event in Mexico. *Geophys. Res. Lett.* 38 (8), L08308. <http://dx.doi.org/10.1029/2011GL047151>.
- Rogers, G., Dragert, H., 2003. Episodic tremor and slip on the Cascadia subduction zone: the chatter of silent slip. *Science* 300 (5627), 1942–1943. <http://dx.doi.org/10.1126/science.1084783>.
- Rubinstein, J.L., Shelly, D.R., Ellsworth, W.L., 2010. Non-volcanic tremor: a window into the roots of fault zones. In: Cloetingh, S., Negendank, J. (Eds.), *New Frontiers in Integrated Solid Earth Sciences*. Springer, Amsterdam, Netherlands, pp. 287–314.

- Samuelson, J., Elsworth, D., Marone, C., 2009. Shear-induced dilatancy of fluid-saturated faults: experiment and theory. *J. Geophys. Res., Solid Earth* 114 (B12), B12404. <http://dx.doi.org/10.1029/2008JB006273>.
- Scholz, C.H., 2002. *The Mechanics of Earthquakes and Faulting*. Cambridge University Press, Cambridge, UK.
- Segall, P., Bradley, A.M., 2012. Slow-slip evolves into megathrust earthquakes in 2D numerical simulations. *Geophys. Res. Lett.* 39 (18), L18308. <http://dx.doi.org/10.1029/2012GL052811>.
- Segall, P., Rubin, A.M., Bradley, A.M., Rice, J.R., 2010. Dilatant strengthening as a mechanism for slow slip events. *J. Geophys. Res.* 115 (B12), B12305. <http://dx.doi.org/10.1029/2010JB007449>.
- Shelly, D.R., 2009. Possible deep fault slip preceding the 2004 Parkfield earthquake, inferred from detailed observations of tectonic tremor. *Geophys. Res. Lett.* 36 (17), L17318. <http://dx.doi.org/10.1029/2009GL039589>.
- Shelly, D.R., 2010a. Periodic, chaotic, and doubled earthquake recurrence intervals on the deep San Andreas Fault. *Science* 328 (5984), 1385–1388. <http://dx.doi.org/10.1126/science.1189741>.
- Shelly, D.R., 2010b. Migrating tremors illuminate complex deformation beneath the seismogenic San Andreas fault. *Nature* 463 (7281), 648–652. <http://dx.doi.org/10.1038/nature08755>.
- Shelly, D.R., 2015. Complexity of the deep San Andreas Fault zone defined by cascading tremor. *Nat. Geosci.* 8 (2), 145–151. <http://dx.doi.org/10.1038/ngeo2335>.
- Shelly, D.R., Hardebeck, J.L., 2010. Precise tremor source locations and amplitude variations along the lower-crustal central San Andreas Fault. *Geophys. Res. Lett.* 37 (14), L14301. <http://dx.doi.org/10.1029/2010GL043672>.
- Shelly, D.R., Johnson, K.M., 2011. Tremor reveals stress shadowing, deep postseismic creep, and depth-dependent slip recurrence on the lower-crustal San Andreas fault near Parkfield. *Geophys. Res. Lett.* 38 (13), L13312. <http://dx.doi.org/10.1029/2011GL047863>.
- Shelly, D.R., Beroza, G.C., Ide, S., Nakamura, S., 2006. Low-frequency earthquakes in Shikoku, Japan, and their relationship to episodic tremor and slip. *Nature* 442 (7099), 188–191. <http://dx.doi.org/10.1038/nature04931>.
- Shelly, D.R., Beroza, G.C., Ide, S., 2007. Non-volcanic tremor and low-frequency earthquake swarms. *Nature* 446 (7133), 305–307. <http://dx.doi.org/10.1038/nature05666>.
- Shelly, D.R., Ellsworth, W.L., Ryberg, T., Haberland, C., Fuis, G.S., Murphy, J., Nadeau, R.M., Bürgmann, R., 2009. Precise location of San Andreas Fault tremors near Cholame, California using seismometer clusters: slip on the deep extension of the fault? *Geophys. Res. Lett.* 36 (1), L01303. <http://dx.doi.org/10.1029/2008GL036367>.
- Shelly, D.R., Peng, Z., Hill, D.P., Aiken, C., 2011. Triggered creep as a possible mechanism for delayed dynamic triggering of tremor and earthquakes. *Nat. Geosci.* 4 (6), 384–388. <http://dx.doi.org/10.1038/ngeo1141>.
- Sieh, K.E., 1978. Central California foreshocks of the great 1857 earthquake. *Bull. Seismol. Soc. Am.* 68, 1731–1749.
- Thomas, A.M., Bürgmann, R., Shelly, D.R., Beeler, N.M., Rudolph, M.L., 2012. Tidal triggering of low frequency earthquakes near Parkfield, California: implications for fault mechanics within the brittle–ductile transition. *J. Geophys. Res.* 117 (B5), B05301. <http://dx.doi.org/10.1029/2011JB009036>.
- Tse, S.T., Rice, J.R., 1986. Crustal earthquake instability in relation to the depth variation of frictional slip properties. *J. Geophys. Res., Solid Earth* 91 (B9), 9452–9472. <http://dx.doi.org/10.1029/JB091iB09p09452>.
- Wech, A.G., Creager, K.C., 2011. A continuum of stress, strength and slip in the Cascadia subduction zone. *Nat. Geosci.* 4 (9), 624–628. <http://dx.doi.org/10.1038/ngeo1215>.
- Wu, C., Shelly, D.R., Gombert, J., Peng, Z., Johnson, P., 2013. Long-term changes of earthquake inter-event times and low-frequency earthquake recurrence in central California. *Earth Planet. Sci. Lett.* 368 (0), 144–150. <http://dx.doi.org/10.1016/j.epsl.2013.03.007>.